High Power Laser Science and Engineering, (2016), Vol. 4, e30, 5 pages.

doi:10.1017/hpl.2016.31

Short-pulse laser-driven x-ray radiography

E. Brambrink[1], S. Baton[1], M. Koenig[1,2], R. Yurchak[1], N. Bidaut[1], B. Albertazzi[1], J. E. Cross[3], G. Gregori[3], A. Rigby[3], E. Falize[4], A. Pelka[5], F. Kroll[5], S. Pikuz[6], Y. Sakawa[7], N. Ozaki[8], C. Kuranz[9], M. Manuel[9], C. Li[10], P. Tzeferacos[11], and D. Lamb[11]

[1]*LULI - CNRS, Ecole Polytechnique, CEA : Université Paris-Saclay; UPMC Univ Paris 06 : Sorbonne Universités - F-91128 Palaiseau cedex, France*

[2]*Institute for Academic Initiatives, Osaka U., Suita, Osaka 565-0871, Japan*

[3]*Clarendon Laboratory, University of Oxford, Parks Road, Oxford OX1 3PU, UK*

[4]*CEA-DAM-DIF, F-91297 Arpajon, France*

[5]*HZDR, Bautzner Landstrae 400, 01328 Dresden, Germany*

[6]*JIHT-RAS, 13-2 Izhorskaya st., Moscow, 125412, Russia*

[7]*Institute of Laser Engineering, Osaka U., Suita, Osaka 565-0871, Japan*

[8]*Graduate School of Engineering, Osaka U., Suita, Osaka 565-0871, Japan*

[9]*Department of Energy Engineering Science, Faculty of Engineering Sciences, Kyushu University, Japan*

[10]*Plasma Science and Fusion Center, Massachusetts Institute of Technology, 77 Massachusetts Avenue, Cambridge, MA 02139, USA*

[11]*Flash Center for Computational Science, University of Chicago, IL 60637, USA*

(Received 30 April 2016; revised 12 July 2016; accepted 3 August 2016)

Abstract

We have developed a new radiography setup with a short-pulse laser-driven x-ray source. Using a radiography axis perpendicular to both long- and short-pulse lasers allowed optimizing the incident angle of the short-pulse laser on the x-ray source target. The setup has been tested with various x-ray source target materials and different laser wavelengths. Signal to noise ratios are presented as well as achieved spatial resolutions. The high quality of our technique is illustrated on a plasma flow radiograph obtained during a laboratory astrophysics experiment on POLARs.

Keywords: laboratory astrophysics; short-pulse laser; x-ray radiography

1. Introduction

Pulsed x-ray radiography allows the study of fast evolving phenomena like shock compression of matter or plasma outflows. Using short-pulse laser-driven x-ray sources with ps pulse duration helps to reduce smearing of even high velocity phenomena ($v > 100\,\mathrm{km\,s^{-1}}$) to the μm scale, making this technique ideal for the highly transient laser-driven compression and hydrodynamics. For example, studying condensed matter at high pressures (≫1 Mbar) is an important field of research due to its outreach for planetary science, inertial confinement fusion and condensed matter physics in general (phase transitions, high pressure chemistry). Laboratory astrophysics studying plasma flows and instabilities using high-energy laser systems have also strongly evolved in the recent years. X-ray radiography is fundamental in these experiments to investigate these flows' temporal evolution as they are often opaque to visible light. The development of high-energy lasers like NIF and LMJ opens new opportunities for experiments and makes the study of these extreme states of matter with this type of diagnostic even more critical. The transient character of all these experiments requires x-ray radiography with high temporal resolution, which allows measuring density distributions, direct density measurements[1], instabilities growth[2] and plasma shapes[3]. Depending on the time evolution of the plasma to be investigated, this diagnostic requires an x-ray source with a short duration (≈1 ps), photon energies in the range of a few keV to > 100 keV and a sufficient large photon number to obtain a radiograph.

Short-pulse (sub-ps to a few ps) high-energy (>J) lasers can produce bright x-ray sources well suited for single shot radiography. When such a laser interacts with a solid sample

Correspondence to: E. Brambrink, LULI - CNRS, Ecole Polytechnique, CEA : Université Paris-Saclay; UPMC Univ Paris 06 : Sorbonne Universités - F-91128 Palaiseau cedex, France.
Email: erik.brambrink@polytechnique.edu

a large number of energetic electrons is generated[4, 5], which propagates into the sample. These electrons will either emit continuous radiation via the Bremsstrahlung process or create K-shell vacancies via impact ionization, which leads to characteristic line emission (K_α and K_β). These electrons and the compensating return current will heat the material, which can ionize it. This can result in radiation from highly ionized states (He_α)[6], but this effect is limited to photon energies of a few keV. The x-ray pulse duration is in the order of the laser pulse duration, thus a few ps in our case. By adjusting the source material and detector filtering, the photon energy for the radiography can be set over a wide range (a few keV to 100 keV). The conversion efficiency from laser light to x-rays is about 10^{-4}–10^{-5}[7], which as an example, can produce 6×10^{13} photons of 10 keV energy emitted isotropically in 4π with a 100 J laser.

X-ray radiography can be achieved in different setups like point-projection geometry, imaging with a pinhole camera or crystal imaging. We used point-projection geometry in our experiment due to its simplicity. In this case, a point like x-ray source projects the sample directly to the detector without use of any imaging system (pinhole camera, spherical crystal or zone plates).

Due to the spreading of the electrons in the x-ray source target, the radiation is emitted from an extended zone (reported values range from 50 μm to 1 mm[8–10]). In order to obtain a smaller source size, which determines the spatial resolution, mass reduced targets are used. Either, one uses the emission from an edge of a foil to restrict the size in one dimension ('1D resolution') or the cross-section of a thin wire ('2D resolution')[11].

A major problem arises in many laser facilities such as LULI2000 or LMJ/PETAL from the geometry of the laser beams (drive beam and backlighter beam) and diagnostic ports. At LULI2000, for example, both laser beams arrive in the equatorial plane of the target chamber at an angle of 112°. In the case of LMJ/PETAL, a 90° angle between the short-pulse laser and the diagnostic axis parallel to the shock direction. The radiography diagnostics are also normally placed in the equatorial plane, either using standard diagnostic ports or mounting. The propagation direction of shocks and plasma flows are fixed by either laser or diagnostic axis and in consequence the direction for the radiography is perpendicular to this axis and close to the axis of the short-pulse laser. As described above, a wire target pointing in the radiography direction is necessary to obtain a good spatial resolution, which thus is at a shallow angle relative to the short-pulse laser beam axis. This angle is not favorable for the radiography due to low x-ray conversion and detector noise due to directed energetic electrons accelerated in laser direction[12]. Changing the angle between the two beams is, due to the size of the beams, a cost intensive operation, involving large optomechanics.

Thus, we have chosen a vertical radiography axis (out of the equatorial plane) (see Figure 1) to avoid all issues

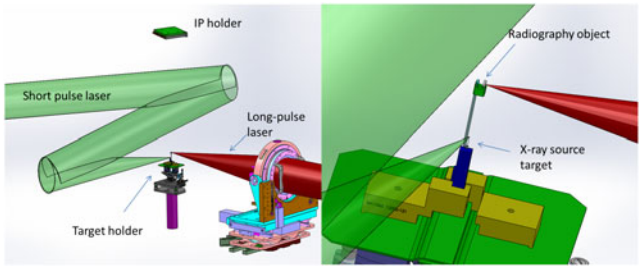

Figure 1. Radiography setup with imaging plate, target holder and laser beams. On the right a magnification of the target holder with x-ray source and radiography sample.

mentioned above and also to test this dedicated geometry that will be the only possible one on LMJ-PETAL. Our new design requires to position the x-ray source target below the sample and the detector above. This allows irradiating the x-ray source target with nearly normal incidence independently of the angle between the drive and backlighter beams, which is the only possibility to reach high signal levels while suppressing noise. This configuration needs important mechanical changes: as the target holder and target manipulator are placed below the sample, space is limited. In the case of LULI2000, the incoming beam to the focussing parabola of the backlighter beam passes through the headroom above the sample, which limits the positions a detector can be placed. In addition, a diagnostic port holding the detector on this axis is necessary.

In this paper we describe the first tests done with this configuration comparing different laser parameters and x-ray sources material with static samples. Then we applied this new scheme to a laboratory astrophysics experiment (POLAR) that has been performed on LULI2000[13]. We illustrate the quality of the radiography technique by looking at the propagation of a high Mach number ($M = 5$–10) plasma flow.

2. Setup

The experiment has been performed on the *LULI2000* facility, using the PICO2000 beam. We used both the fundamental wavelength (1053 nm) and frequency doubled (527 nm) with the energies on target of 40 and 25 J, respectively. The beam was used at best compression (1.5 ps) with a ns ASE contrast better than 10^{-6} and discrete prepulse suppression better than 10^{-5}. When used in the frequency doubled mode, three dichroic mirrors after the doubling crystal suppressed the fundamental wavelength and improve the contrast. The laser was focussed to 8 μm (best focus) when operated frequency doubled and defocussed to 50–100 μm to comply with radiation safety rules.

The x-ray source targets were thin metallic wires pointing in the vertical direction to obtain a good spatial resolution

in two dimensions. Target materials were V, Cu, Mo and W with K_α energies of 4.95, 8.04, 17.4 and 58 keV, respectively. It is important to point out that even for the low-Z (V and Cu) species lines of ionized states are expected (He-like ions). The diameter of the wires was either 10 μm (W and Mo) or 20 μm (V and Cu).

To characterize the x-ray source, we used several diagnostics. The spatial resolution was measured with a 400 lines per inch, 10 μm thick gold grid, which was positioned 23.5 mm from the x-ray source on the vertical axis. This corresponds to the target chamber center, where the ns beam is generally focussed and the sample will be placed in later experiments.

The detector for the radiography is a 100 mm × 100 mm imaging plate (IP)[14] placed at a distance of 588 mm from the x-ray source, resulting in a 25× magnification of the grid projection. The detector was covered with a 13 μm thick Al foil to protect the IP from visible light. In addition, we placed an Al and plastic step wedge in front of the detector to estimate the dynamic resolution of the radiography and spectral composition of the source. In this configuration, the IP is sensitive to x-rays over the complete spectrum above ≈2 keV, which includes Bremsstrahlung and, in the case of Mo and W, also L-band radiation.

In order to characterize the spectral distribution, we used a crystal spectrometer in von-Hamos geometry covering the K-shell radiation of V and a transmission crystal spectrometer for the Mo K-shell radiation. Thus, for these elements we obtain independent data on the line emission.

3. Results

With the described setup we obtained high-quality radiographs. A typical raw data is shown in Figure 2. This result was very reproducible, out of 17 shots only one showed a much weaker signal, most likely due to a pointing problem of the laser. The raw data shows several features important for a proper density diagnostic. The unperturbed signal is homogeneous over the detector with a low noise level, which is necessary to calculate correctly the absorption at different places. The plastic step wedge shows distinct zones important for the dynamic resolution of the signal, leading to small errors in the density calculation.

We analyzed the total signal S on the IP in function on the laser wavelength. Generally, the IP signal has a statistical noise after readout in the order of $\sqrt{S}$. Thus, a high signal is necessary for reducing the (relative) noise. We averaged the signal for two distinct regions: outside of the grid to obtain the total signal arriving on the detector and behind the outer ring of the grid, which corresponds to the transmission through 10 μm of gold, considered to be background signal from high-energy photons. The noise of this background contributes to the error in absorption measurement, thus a low background signal is beneficial. The results are summarized in Table 1.

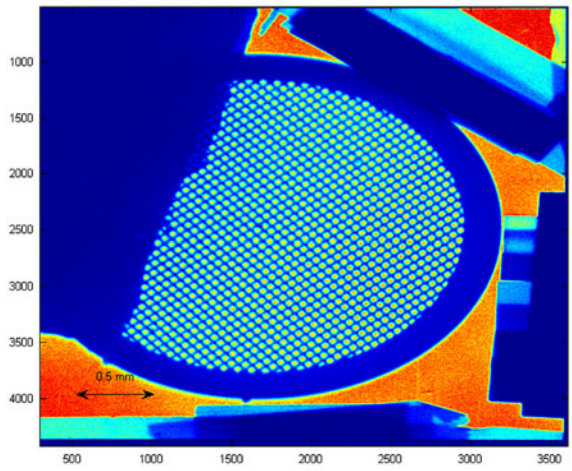

Figure 2. Raw data of the radiography. The projected object is a 400 lpi gold grid. In addition, there are step targets of plastic and aluminum to estimate the dynamic resolution.

Table 1. Comparison of x-ray signals from different materials and for two laser wavelengths. The background is measured behind the edge of the gold grid.

	ω		2ω	
	Signal	Background	Signal	Background
V	11.7	2.7	58	4
Cu	3.7	0.9	11	0.6
Mo	9	1.5	20	2.2

We see in all cases a strong increase of the signal using the frequency doubled laser although the laser energy was lower, while the increase of the background signal is less pronounced or even reduced. As the laser intensity was higher in the case of frequency doubling (smaller focus), it is not clear, if this is only due to the laser wavelength and prepulse reduction or if there is also an intensity effect. It is also not clear, which spectral components are responsible for this increase. For V and Mo, where we also measured line radiation, we observed only for Mo an increase in line radiation, which was still less than the spectrally integrated signal on the IP. However, the signal to background ratio was, for frequency doubled laser light, in all cases better.

With changing the laser wavelength, we observed also a strong change in the spectral shape of the emitted x-rays from V samples. While the emission from ionized states (He_α) is dominant using the laser at fundamental wavelength, it shifts to K_α radiation for frequency doubled light (see Figure 3) resulting in a narrower spectrum.

This is even more surprising, as the laser intensity was higher, which should heat the sample and favorites emission from ionized states[6]. Thus frequency doubling reduces target heating. Whether this is due to prepulse suppression or changes in the electron energy distribution due to the wavelength needs further investigation.

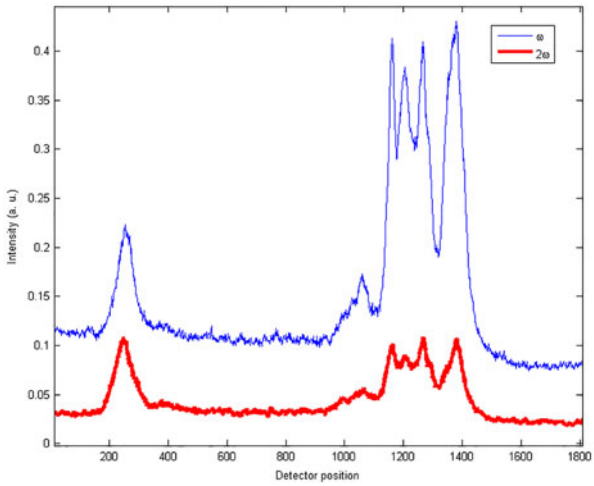

Figure 3. V spectrum in function of the laser wavelength. The He-like lines are reduced compared to the K_α line.

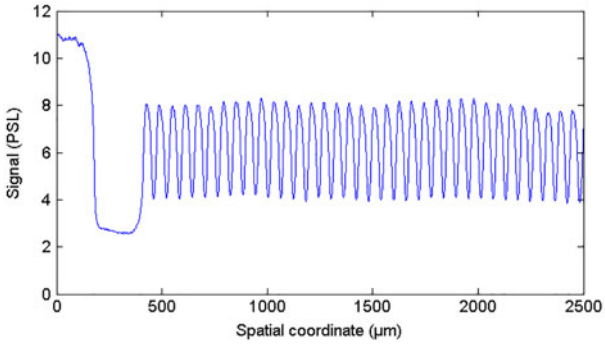

Figure 4. Signal profile through the grid region, showing the unperturbed signal, the edge of the grid and the oscillations of the grid. Note the small variations of the signal over the detector.

Using wire targets for radiography along the wire axis, a spatial resolution in the order of the source size, i.e., the diameter of the wire, is expected. We verified this with the grid sample shown in Figure 2. The grid has 400 line pairs per inch, thus 15.7 line pairs mm^{-1}. This corresponds to a distance of 64 μm from the beginning of one bar to the next, thus the bar is approximately 32 μm width. From a line-out like in Figure 4 we can measure the contrast. On the left side of Figure 4, the line-out starts with the unperturbed signal, followed by a large gap, which corresponds to the ring around the grid. The signal measured here was considered to be background from high-energy photons and subtracted from the signal. The following oscillations correspond to the grid, where the reduction in contrast can be associated with the spatial resolution.

For the line-out in Figure 4 we obtain a contrast of 0.5. We have observed contrasts between 0.5 and 0.8 throughout the experiment, indicating spatial resolutions better than 30 μm.

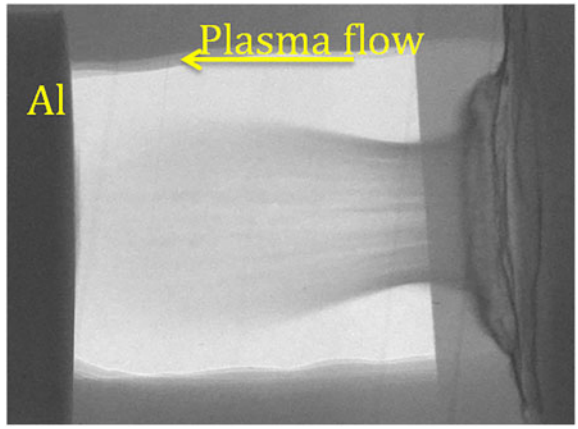

Figure 5. X-ray radiograph at 5.1 keV (V backlighter) taken 75 ns after the main drive beam.

The edge function of the ring around the grid is in agreement with this finding. As mentioned above, the x-ray signal is composed of different photon energies. It is possible, that different photon energies have different source sizes, thus relating the contrast with a spatial resolution might be complicated. However, resolving the grid structures of ≈30 μm indicates a spatial resolution better than this.

We have demonstrated the radiography capabilities in a POLAR experiment, conducted few months later. The Polar experiment consisted to observe the propagation of a high Mach number plasma flow, generated by a strong shock breaking out in the vacuum, and its impact on a solid obstacle (1 mm thick aluminum) located around 2.5 mm away. This target scheme mimics the situation in the so-called POLAR astrophysical objects. Here a main heavy star (white dwarf) accretes matter from a companion star. The matter flow between the stars is collimated due to a high magnetic field ($B > 10$ MG). The impact on the white dwarf corresponds to the impact on the obstacle in the experiment. In Figure 5, we can clearly observe the plasma flow that propagates from the main target to the obstacle (from right to left). The impact of the flow generates a reverse shock that we infer in front of the aluminum obstacle. Finally, we clearly observe small scale structures (a few tens of μm) that show the quality of this radiograph.

4. Summary

We have demonstrated successfully reproducible high-quality x-ray radiography in a new configuration of x-ray source and detector. Spatial resolutions better than 30 μm have been achieved. The data indicates a better signal to background ratio using frequency double laser light, although the difference is not important for the quality of the radiography. There are open questions about the spectral composition of the radiation recorded by the detector,

especially about the contribution of continuous radiation. Although the resulting ambiguity of the absorption can be overcome by an in situ calibration, the underlying physics exhibits some interest (ionization distribution, electron distribution). A detailed measurement of the spectral distribution would be a benefit. Finally an example on a laboratory astrophysics experiment demonstrated the high resolution obtained with this configuration.

Acknowledgments

S.A. Pikuz acknowledges the support of RFBR grant 14-29-06099 and Competitiveness Programme of NRNU MEPhI.

References

1. E. Brambrink, H. G. Wei, B. Barbrel, P. Audebert, A. Benuzzi-Mounaix, T. Boehly, T. Endo, C. D. Gregory, T. Kimura, R. Kodama, N. Ozaki, H.-S. Park, and M. Koenig, Phys. Rev. E **80**, 056407 (2009).
2. K. T. Lorenz, M. J. Edwards, S. G. Glendinning, A. F. Jankowski, J. McNaney, S. M. Pollaine, and B. A. Remington, Phys. Plasmas **12**, 056309 (2005).
3. T. R. Dittrich, S. W. Haan, M. M. Marinak, S. M. Pollaine, D. E. Hinkel, D. H. Munro, C. P. Verdon, G. L. Strobel, R. McEachern, R. C. Cook, C. C. Roberts, D. C. Wilson, P. A. Bradley, L. R. Foreman, and W. S. Varnum, Phys. Plasmas **6**, 2164 (1999).
4. F. Pisani, A. Bernardinello, D. Batani, A. Antonicci, E. Martinolli, M. Koenig, L. Gremillet, F. Amiranoff, S. Baton, J. Davies, T. Hall, D. Scott, P. Norreys, A. Djaoui, C. Rousseaux, P. Fews, H. Bandulet, and H. Pepin, Phys. Rev. E **62**, R5927 (2000).
5. S. P. Hatchett, C. G. Brown, T. E. Cowan, E. A. Henry, J. S. Johnson, M. H. Key, J. A. Koch, A. Bruce Langdon, B. F. Lasinski, R. W. Lee, A. J. Mackinnon, D. M. Pennington, M. D. Perry, T. W. Phillips, M. Roth, T. Craig Sangster, M. S. Singh, R. A. Snavely, M. A. Stoyer, S. C. Wilks, and K. Yasuike, Phys. Plasmas **7**, 2076 (2000).
6. W. Theobald, K. Akli, R. Clarke, J. A. Delettrez, R. R. Freeman, S. Glenzer, J. Green, G. Gregori, R. Heathcote, N. Izumi, J. A. King, J. A. Koch, J. Kuba, K. Lancaster, A. J. MacKinnon, M. Key, C. Mileham, J. Myatt, D. Neely, P. A. Norreys, H.-S. Park, J. Pasley, P. Patel, S. P. Regan, H. Sawada, R. Shepherd, R. Snavely, R. B. Stephens, C. Stoeckl, M. Storm, B. Zhang, and T. C. Sangster, Phys. Plasmas **13**, 043102 (2006).
7. H.-S. Park, D. M. Chambers, H.-K. Chung, R. J. Clarke, R. Eagleton, E. Giraldez, T. Goldsack, R. Heathcote, N. Izumi, M. H. Key, J. A. King, J. A. Koch, O. L. Landen, A. Nikroo, P. K. Patel, D. F. Price, B. A. Remington, H. F. Robey, R. A. Snavely, D. A. Steinman, R. B. Stephens, C. Stoeckl, M. Storm, M. Tabak, W. Theobald, R. P. J. Town, J. E. Wickersham, and B. B. Zhang, Phys. Plasmas **13**, 056309 (2006).
8. R. B. Stephens, R. A. Snavely, Y. Aglitskiy, F. Amiranoff, C. Andersen, D. Batani, S. D. Baton, T. Cowan, R. R. Freeman, T. Hall, S. P. Hatchett, J. M. Hill, M. H. Key, J. A. King, J. A. Koch, M. Koenig, A. J. MacKinnon, K. L. Lancaster, E. Martinolli, P. Norreys, E. Perelli-Cippo, M. Rabec Le Gloahec, C. Rousseaux, J. J. Santos, and F. Scianitti, Phys. Rev. E **69**, 066414 (2004).
9. K. L. Lancaster, J. S. Green, D. S. Hey, K. U. Akli, J. R. Davies, R. J. Clarke, R. R. Freeman, H. Habara, M. H. Key, R. Kodama, K. Krushelnick, C. D. Murphy, M. Nakatsutsumi, P. Simpson, R. Stephens, C. Stoeckl, T. Yabuuchi, M. Zepf, and P. A. Norreys, Phys. Rev. Lett. **98**, 125002 (2007).
10. J. F. Seely, C. I. Szabo, P. Audebert, E. Brambrink, E. Tabakhoff, and L. T. Hudson, Phys. Plasmas **17**, 023102 (2010).
11. H.-S. Park, B. R. Maddox, E. Giraldez, S. P. Hatchett, L. T. Hudson, N. Izumi, M. H. Key, S. Le Pape, A. J. MacKinnon, A. G. MacPhee, P. K. Patel, T. W. Phillips, B. A. Remington, J. F. Seely, R. Tommasini, R. Town, J. Workman, and E. Brambrink, Phys. Plasmas **15**, 072705 (2008).
12. E. Brambrink, H. G. Wei, B. Barbrel, P. Audebert, A. Benuzzi-Mounaix, T. Boehly, T. Endo, C. Gregory, T. Kimura, R. Kodama, N. Ozaki, H.-S. Park, M. Rabec le Gloahec, and M. Koenig, Phys. Plasmas **16**, 033101 (2009).
13. E. Falize, A. Ravasio, B. Loupias, A. Dizire, C. D. Gregory, C. Michaut, C. Busschaert, C. Cavet, and M. Koenig, High Energy Density Physics **8**, 1 (2012).
14. M. Sonoda, M. Takano, J. Miyahara, and H. Kato, Radiology **148**, 833 (1983).